LAWRENCE
LIVERMORE
NATIONAL
LABORATORY

UCRL-JRNL-205965

Transcription-Driven Twin Supercoiling of a DNA Loop: A Brownian Dynamics Study

S. P. Mielke, W. H. Fink, K. Krishnan, N. Gronbech-Jensen, C. J. Benham

August 11, 2004

Journal of Chemical Physics

Transcription-driven twin supercoiling of a DNA loop: A Brownian dynamics study

Steven P. Mielke[1,2,*], V.V. Krishnan[2], Niels Grønbech-Jensen[3], Craig J. Benham[4], and William H. Fink[5]

[1]Biophysics Graduate Group, University of California, Davis, CA 95616; [2]Molecular Biophysics Group, L-448 Biology and Biotechnology Research Program, Lawrence Livermore National Laboratory, Livermore, CA 94551; [3]Department of Applied Science, UC Davis; [4]UC Davis Genome Center, UC Davis; and [5]Department of Chemistry, UC Davis

The torque generated by RNA polymerase as it tracks along double-stranded DNA can potentially induce long-range structural deformations integral to mechanisms of biological significance in both prokaryotes and eukaryotes. In this report, we introduce a dynamic computer

*To whom correspondence should be addressed. E-mail: smielke@lifshitz.ucdavis.edu.

model for investigating this phenomenon. Duplex DNA is represented as a chain of hydrodynamic beads interacting through elastic potentials. The chain, linear when relaxed, is looped to form two open but topologically constrained subdomains. This permits the dynamic introduction of torsional stress via a centrally applied torque. We simulate by Brownian dynamics the 100 μs response of a 477-basepair B-DNA template to the localized torque generated by the prokaryotic transcription ensemble. Following a sharp rise at early times, the distributed twist assumes a nearly constant value in both subdomains, and a succession of supercoiling deformations occurs as superhelical stress is increasingly partitioned to writhe. The magnitude of writhe surpasses that of twist before also leveling off when the structure reaches mechanical equilibrium with the torsional load. Superhelicity is simultaneously right-handed in one subdomain and left-handed in the other. The properties of the chain at the onset of writhing agree well with predictions from theory, and the generated stress is ample for driving secondary structural

transitions in physiological DNA. These results suggest that the torsional stress generated by transcription can significantly deform the DNA template over short times. This highlights the potential of transcription and other tracking processes to play a central role in gene regulation, and prompts further investigation of dynamically-generated supercoiling.

The topology of double-stranded DNA (dsDNA) plays a significant role in the processes by which this macromolecule carries out its biological functions. The superhelical stress produced when the twin sugar-phosphate backbones of duplex DNA are either over- or underwound, relative to their relaxed winding value (approximately one turn per 10.5 base-pairs (bp) for B-form DNA under physiological conditions), leads to both global and localized structural deformations that are often prerequisite to such fundamental processes as replication, transcription, recombination, and repair in both prokaryotes and eukaryotes (see, for example, Ref. [1]). These deformations are a consequence of the coupling of molecular

twist and writhe, as quantified by the expression [2]:

$$Lk = Tw + Wr. \tag{1}$$

Here, Lk represents the linking number (roughly speaking, the number of times one backbone "links through," or winds around, the other), Tw represents the helical twist (the number of times either backbone winds around the helix axis), and Wr represents the writhe, or degree of supercoiling (the number of signed crossings of the helix axis in planar projection, averaged over all projection directions). Though Lk is strictly defined only for topologically closed DNA—*i.e.*, for closed circular DNA (ccDNA) or anchored linear DNA—it is in practice also a relevant descriptor of, for example, regions of free linear DNA much longer than the persistence length (approximately 500Åfor B-DNA). In such regions, considerable stress can accrue upon torsional loading, due to the resistance of natural bends to translation through a viscous medium [3]. For a given molecule, the superhelical stress produced by deviations of Lk from its relaxed value, Lk_0, is accommodated

by changes in Tw, Wr, or both:

$$\Delta Lk = (Lk - Lk_0) = \Delta Tw + \Delta Wr. \qquad (2)$$

Here, ΔTw corresponds to localized, sequence-dependent twist deformations such as strand separation, cruciform extrusion, and B-to-Z transition, as well as to continuously distributed overtwist or undertwist. Superhelical stress-induced strand separation in promoter regions of both prokaryotic and eukaryotic genomes, for example, is implicated in the initiation of transcription [4]. ΔWr corresponds to bend (supercoiling) deformations, which are integral, for example, to site-specific recombination events [5].

Processes that alter DNA topology are inherently dynamic in character. A well known example is the tracking of RNA polymerase (RNAP) along the double helix during transcription. This mechanism requires counter-rotation of RNAP (along with its RNA transcript and any associated proteins) relative to the DNA template, because of the latter's helical geometry. Under a variety of circumstances, rotation of RNAP is hindered, producing a torque capable of substan-

tially supercoiling the template [3, 6–9]. One such scenario, a transcription-induced twin-supercoiled-domain, is illustrated in Figure 1, which was adapted from Reference [6]. In Fig. 1*a*, a transcription ensemble, $\mathcal{T}$, tracks from left to right along a linear DNA template with ends anchored to large cellular structures [8] (broken horizontal bars attached to solid squares in the figure). The ensemble includes an elongating RNA transcript. Anchoring and/or frictional resistance preventing rotation of $\mathcal{T}$ within the cellular milieu leads instead to local rotation of the template under an applied torque, represented by the circular arrow in the center of Fig. 1*b* and *c*. This rotation relative to the anchored ends produces superhelical stress throughout the domain, generating positive supercoils ($\Delta Lk > 0$) downstream, and negative supercoils ($\Delta Lk < 0$)upstream, from $\mathcal{T}$ (Fig. 1*c*), and potentially also driving localized, sequence-dependent duplex transitions, such as strand separation, required for such regulatory events as initiation of replication within the domain. Exploration of the twin domain phenomenon, for which there is now exten-

sive experimental support (reviewed in Ref. [10]), continues to be an active area of research (see, *e.g.*, Refs. [11–13]).

Here, we present a dynamic model of the transcription-driven formation of a twin-supercoiled domain. Our approach is based on a method for large-scale, long-time dynamics, whereby dsDNA is represented as a chain of discrete, spherical beads that interact through Hookean elastic potentials [14–16]. The physical size of the beads is set according to the hydrodynamic diameter of DNA, so that each bead represents several basepairs. The presence of transcriptionally active but anchored RNAP is represented by an external torque that spans a region of approximately the same extent as the footprint of prokaryotic RNAP. The magnitude of this torque is chosen according to experimental measurements of the force generated by *E. coli* RNAP against an opposing load [3, 17]. With this representation, the positions and twist angles of beads in the chain are time-evolved using Brownian dynamics (BD); *i.e.*, simulations based upon numerical integration of overdamped equations of motion [18]. BD incor-

porates DNA-solvent interaction effects via inherent dissipative and stochastic forces, rather than explicit inclusion of hundreds or thousands of solvent molecules. Twist-bend coupling, which allows the model to capture the effects of superhelicity upon the dynamics, enters through a set of torsional forces that result from the independence of the infinitesimal coordinates of the beads [15, 19]. The BD bead-chain representation of dsDNA has, for equilibrium systems involving free linear DNA and statically-stressed superhelical ccDNA, predicted with reasonable accuracy such observable parameters as decay anisotropy measured by fluorescence depolarization and triplet anisotropy decay [14], translational and rotational diffusion coefficients measured by dynamic light scattering [15], and ring closure probablities measured in cyclization reaction experiments [20]. Our results demonstrate that the present model captures several significant features of transcriptional twin supercoiling, and, more generally, elucidates the nonequilibrium response of DNA to dynamically imposed torsional stress, suggesting its potential as a tool

for analysis of solvent-mediated dynamic supercoiling under a wide range of conditions and circumstances.

Methods

Model. We model DNA as a chain of N rigid spheres (beads) connected by $N-1$ virtual bonds of equilibrium length b_0. The instantaneous configuration of the chain is then described by a set of bead position vectors, $\{\mathbf{r}_i\}_{i=1,N}$, and a set of body-fixed coordinate (bfc) unit vectors, $\{\hat{u}_i, \hat{f}_i, \hat{v}_i\}_{i=1,N-1}$, defining local orthogonal coordinate frames, in which $\hat{u}_i \equiv \frac{\mathbf{r}_{i+1}-\mathbf{r}_i}{|\mathbf{r}_{i+1}-\mathbf{r}_i|}$, $\hat{f}_i$ is defined in a direction orthogonal to $\hat{u}_i$, and used to track the twist, and then $\hat{v}_i \equiv \hat{u}_i \times \hat{f}_i$. Contiguous bfc frames are connected by standard Euler transformation matrices [21], in which the Euler angles, α_i, β_i, and γ_i, are expressed in terms of the bfc vectors [14]. Bead-bead interactions are then characterized by the following elasto-harmonic potentials of stretching, bending, and twisting, respectively:

$$U_s(b_i) = \frac{k_B T}{2\delta^2}(b_i - b_0)^2 \quad (3)$$

$$U_b(\beta_i) = \frac{k_B T}{2\psi^2}(\beta_i - \beta_0)^2 \quad (4)$$

$$U_t(\alpha_i + \gamma_i) \;=\; \frac{k_B T}{2\xi^2}(\alpha_i + \gamma_i - \Phi_0)^2. \qquad (5)$$

Here, $\frac{k_B T}{\delta^2}$, $\frac{k_B T}{\psi^2}$, and $\frac{k_B T}{\xi^2}$ represent elastic coefficients, in which k_B is Boltzmann's constant and T is the absolute temperature. The choice of values for the parameters, δ, ψ, and ξ, will be discussed below. In Equation (3), $b_i = |\mathbf{r}_{i+1} - \mathbf{r}_i|$. In Equations (4) and (5), β_0 and Φ_0 are the equilibrium bend and twist angles, respectively, between adjacent beads. Both β_0 and Φ_0 are set to zero throughout this work. (Setting $\Phi_0 = 0$ in turn sets $Lk_0 = 0 \Rightarrow Lk = \Delta Lk$.) The form of the potentials expressed by Equations (3)–(5) assumes both homogeneity and isotropic stretching, bending, and twisting of the chain.

In addition to the potentials (3)–(5), we include an excluded volume potential of the form

$$\begin{aligned} U_{\mathrm{EV}}(r_{ij}) &= 4\varepsilon k_B T \left[\left(\frac{\sigma_{\mathrm{EV}}}{r_{ij}} \right)^{12} - \left(\frac{\sigma_{\mathrm{EV}}}{r_{ij}} \right)^{6} \right], \quad (r_{ij} < \sqrt[6]{2}\sigma_{\mathrm{EV}}) \\ U_{\mathrm{EV}}(r_{ij}) &= 0, \quad (r_{ij} \geq \sqrt[6]{2}\sigma_{\mathrm{EV}}), \end{aligned} \qquad (6)$$

where r_{ij} is the distance between the ith and jth bead centers, and ε and σ_{EV} are the usual Lennard-Jones (LJ) parameters,

corresponding to the depth and r_{ij}-intercept of the LJ potential function, respectively. The quantity $\sqrt[6]{2}\sigma_{\mathrm{EV}}$ demarcates the value of r_{ij} corresponding to the minimum of the LJ well. The quantity σ_{EV} is then set so that this value coincides with the equilibrium separation of adjacent beads, b_0. The presence of U_{EV} prevents the chain from self-crossing. In that unphysical event, Lk would not be conserved, as the chain would be able to relieve superhelical stress by passing through itself. The forces and torques needed to time-evolve the chain in the presence of solvent are derived from the expressions represented by Equations (3)–(6). Electrostatic interactions are not explicitly considered.

Molecular System. The radius of each bead in a 50-bead chain is set equal to the hydrodynamic radius of B-DNA. We use the value $R_{\mathrm{HYD}} = 15.92$Å [23], corresponding to approximately 4.68 3.4Åbasepair steps. Each bead then represents approximately 9.36 bp. The equilibrium separation between bead centers, b_0, is set at $2R_{\mathrm{HYD}}$, so that the beads "touch" when $b = b_0$.

In order to represent anchoring of the chain due to interaction with an effectively immobile protein complex ($\mathcal{T}$ in Fig. 1), the two central beads are held translationally fixed throughout our simulations. (It is assumed that neither the complex nor the template actually translocates over the relatively short duration ($\sim\mu$s) of these simulations.) The central beads are also uncoupled, so that each experiences no force or torque due to interaction with the other, and the region between them represents "uncoupled" dsDNA; for example, the locally denatured DNA forming the "transcription bubble" characterizing elongation [24]. Since these beads are spatially fixed and noninteracting, the size of this region (the separation between them) is arbitrary. We set that separation to $4R_{\rm HYD} = 2b_0$, corresponding to the approximately 15–20 bp extent of strand separation in the prokaryotic transcription bubble [24]. Though the center beads are spatially fixed, each remains free to rotate about its local axis vector, $\hat{u}$.

Anchoring of the ends of the chain, represented by attachment to solid squares in Fig. 1, is accomplished by for-

bidding both translation and rotation of the two end beads. These conditions, together with the condition that the two center beads remain translationally fixed, topologically constrain each half of the total structure, so that rotation of beads near the center relative to those at the ends applies superhelical stress throughout the domain. This rotation is effected by applying to the chain a torque external to that arising from the relative twist of adjacent beads. This torque is assumed to be time-independent and unidirectional over time intervals $\sim\mu$s. The chosen form of the external torque is, for each half of the structure, the Gaussian:

$$\tau_{\rm ext} = K_\tau \exp\left[\frac{-(i-i_c)^2}{3.56}\right], \qquad (7)$$

where i_c represents either center bead, and i indexes all other beads in the corresponding half of the chain (with the exception of the end beads, which are restricted from responding to torques). The constant, K_τ, the maximum value of $\tau_{\rm ext}$, is set at the value 1.0×10^{-20}N-m, corresponding to the torque *E. coli* RNA polymerase exerts against a torsional load [3, 17]. The denominator in the argument of the exponential corre-

sponds to a standard deviation, $\sigma = 1.3\bar{3}$ beads. Then 3σ corresponds to approximately 37 bp, and the whole spatial distribution of torques along the chain, in addition to the approximately 18 bp region separating the two center beads, can be (loosely) connected with the footprint of the prokaryotic transcription complex [25]. We choose Equation (7) as the form of the supercoiling torque for its convenience, and do not claim it necessarily represents the actual form of the torque exerted by the transcription ensemble upon the DNA template during transcription.

Numerical Procedure: Initial Conformation. For convenience, since the system is uncoupled in the middle of the chain, each of the two center beads is chosen as the first unit in a circular subchain that lies in the xz-plane, and extends out to one end of the whole structure. This produces an "8-shaped" structure, in which the first and last bead centers in each subchain are separated by a distance b_0. The open chain is looped in this manner as a convenient way in which to provide the spatial degrees of freedom required for potential

writhing deformations induced by the applied torque. This structure also lends itself to extensions of the model to ccDNA studies. One might consider this situation analogous to a biological system in which a linear region of DNA loops as a result of the interaction of proteins with which it is bound; such interactions may even involve the transcription ensemble itself [7]. From the initial positions of the beads, the initial $\hat{u}_i$ are assigned. The initial $\hat{f}_i$ are defined all to point in the $+y$-direction, and then $\hat{v}_i \equiv \hat{u}_i \times \hat{f}_i$.

Time Evolution. Time evolution of the initial system is carried out via an algorithm based on the following set of equations:

$$\mathbf{r}_i(t+\delta t) = \mathbf{r}_i(t) + \frac{D_t}{k_B T}\mathbf{F}_i(t)\delta t + \mathbf{R}_i(t) \quad (8)$$

$$\phi_i(t+\delta t) = \phi_i(t) + \frac{D_r}{k_B T}T_i(t)\delta t + f_i(t). \quad (9)$$

Eq. (8) is a 1st-order Brownian dynamics expression [22] for time evolution of the position of the ith particle in an N-particle system in the diffusive regime, in which damping due to particle-solvent interactions dominates the dynamics [18].

Eq. (9) is the angular analog of Eq. (8) [26]. Together, these expressions allow computation of the position and twist angle of particle i, after a time step of size δt, based on current information. In Eq. (8), $\mathbf{r}_i$ represents the position of particle i in the fixed, global frame, D_t represents its translational diffusion coefficient (assumed to be identical for all beads), $k_B T$ is the thermal energy, $\mathbf{F}_i$ represents the total force acting on particle i, and $\mathbf{R}_i$ represents a stochastic displacement, due to the heat bath, characterized by $<\mathbf{R}_i>= 0$ and $<\mathbf{R}_i^2>= 2D_t\delta t$ [27]. In Eq. (9), ϕ_i represents the twist angle of particle i relative to the local helix axis (the instantaneous $\hat{u}_i$), D_r represents its rotational diffusion coefficient (assumed to be identical for all beads), T_i represents the total torque acting on particle i, and f_i represents a stochastic rotation, again due to the thermal bath, and characterized by $<\phi_i>= 0$ and $<\phi_i^2>= 2D_r\delta t$. Expressions for the elastic and excluded volume contributions to $\mathbf{F}_i$ and T_i are obtained by taking the negative gradients of the potentials expressed by Equations (3)–(6) [14, 15, 19]. The total torque, T_i, addi-

tionally includes a contribution from the external torque, $\tau_{\rm ext}$, expressed by Eq. (7).

Input Parameters. For the parameters δ, ψ, and ξ, which set the values of the force constants in Equations (3)–(5), we use values recommended by Chirico and Langowski for a homogeneous, discrete-chain representaion of B-DNA characterized by isotropic bending [15]. The stretching parameter, δ, corresponds to the fluctuation of the average bead-to-bead distance, and is chosen according to the expression $\delta = 0.008 b_0$. The bending parameter, ψ, is chosen according to its relation to the equilibrium bead-to-bead separation and the persistence length of B-DNA; *i.e.*, $\psi^2 = b_0/500\text{Å}$. The twisting parameter, ξ, is chosen according to the expression for the torsional rigidity, $C_t = \frac{b_0 k_{\rm B} T}{\xi^2}$, with $C_t = 2.6 \times 10^{-28}$J-m. For the excluded volume parameters, we select $\epsilon = 100.0$, for which $U_{\rm EV} = k_{\rm B}T$ when $r_{ij} = 0.165\sigma_{\rm EV}$, and $\sigma_{\rm EV}$ such that the separation corresponding to the minimum of the potential well, $r_{ij} = \sqrt[6]{2}\sigma_{\rm EV}$, coincides with b_0, and the beads experience a mutually repulsive excluded volume force only for separa-

tion values $b < b_0$. We choose a physiological temperature of $T = 310$K and solvent viscosity $\eta = 0.01$Poise. This value of η corresponds to that of bulk water at $T = 293$K, but is retained in our simulations at higher temperature in order to account more realistically for the viscosity of the intracellular environment [28]. The values of the rotational and translational diffusion coefficients are derived from the expressions $D_{\rm rot} = \frac{k_{\rm B}T}{\pi\eta R_{\rm HYD}^2 b_0}$ and $D_{\rm trans} = \frac{k_{\rm B}T}{6\pi\eta R_{\rm HYD}}$, respectively. The results presented here were obtained by taking $N_{\delta t} = 20 \times 10^6$ time steps, with $\delta t = 5$ ps.

Extracted Quantities. In order to quantify the dynamic response of the system, we calculate values of the linking number, twist, and writhe during the course of the simulation, using the expressions

$$4\pi Wr = \sum_j \sum_{i \neq j} [(\mathbf{r}_{j+1} - \mathbf{r}_j) \times (\mathbf{r}_{i+1} - \mathbf{r}_i)] \cdot \frac{(\mathbf{r}_j - \mathbf{r}_i)}{|\mathbf{r}_j - \mathbf{r}_i|^3} \quad (10)$$

$$2\pi Tw = \sum_{i=1}^{N-2} (\alpha_i + \gamma_i). \quad (11)$$

Lk is calculated from the expression $Lk = Tw + Wr$. Equations (10) and (11) are discretizations of White's integral ex-

pressions for Tw and Wr [2]. The dot product in Eq. (10) determines the magnitude of relative nonplanar bending of the segments of the helix axis defined by the pair of axis vectors, $(\mathbf{r}_{i+1}-\mathbf{r}_i)$ and $(\mathbf{r}_{j+1}-\mathbf{r}_j)$. The instantaneous total writhe of each substructure is found by summing over all pairs. We calculate the total writhe for each substructure every 1000 time steps, as well as the time-averaged values of the argument in Eq. (10), separately for each pair of beads, over every 1-μs interval for the first 25 μs of the simulation (results discussed below). The argument in Eq. (11) is the same Eulerian twist angle between bead centers i and $i+1$ found in Eq. (5). The instantaneous total twist of each substructure is found by summing over all beads for which this angle is defined. As with writhe, we calculate the total twist for each substructure every 1000 time steps, and time-averaged values of the argument in Eq. (11), separately for each interbead angle, for each of the first 25 1-μs intervals. Using the calculated values of Lk, we also approximate the superhelical density, $\sigma^{+/-}$, over the length of the structure, throughout the simulation. The

superhelical density is defined as

$$\sigma^{+/-} \equiv \frac{\Delta Lk}{Lk_0}, \tag{12}$$

where $\Delta Lk = Lk$ is the linking difference, which determines the sign of σ, and Lk_0 is the relaxed linking number, given by $N/10.5$, in which N is the number of basepairs (234) in each 25-bead subdomain, and 10.5 is the number of base pairs per helical repeat of unstressed B-DNA.

All simulations were performed on a Silicon Graphics workstation, using C codes (including Numerical Recipes routines [29]) and Perl scripts. Trajectory visualizations were generated with Visual Molecular Dynamics (VMD) [30], which is freely available at http://www.ks.uiuc.edu/Research/vmd/.

Results and Discussion

Fig. 2 shows six snapshots from the first 25 μs of a 100 μs trajectory obtained from the BD procedure described above. The simulation time to which each snapshot corresponds is indicated. The tube in the figure represents the approximately 477 bp domain of modeled B-DNA. The central orange seg-

ment represents the approximately 18 bp uncoupled region between the two spatially fixed center beads. The domain is linear when relaxed ($\beta_0 = 0$ for all subunits), but is fixed in a "double-loop" to permit supercoiling due to the continually applied torque and imposed constraints. As the simulation proceeds, each half of the initially polygonal structure (Fig. 2*a*) is seen to undergo a succession of plectonemic writhing deformations, in which torsional strain energy is converted to bending strain energy through the twist-bend coupling explicitly expressed by the equations of motion of the system. The results of the total Lk, Tw, and Wr calculations described in Methods are shown in Fig. 3, where it can be seen that the imposed superhelical stress is positive in one half of the structure (hereafter called $\mathcal{S}^+$), and negative in the other ($\mathcal{S}^-$), as expected for the twin supercoiling scenario illustrated in Fig. 1.

Fig. 3 shows that, initially, $Wr \approx 0$, and $Lk(t) = \Delta Lk(t)$ is manifested almost entirely as a sharp rise in $|Tw|$ in both subdomains as torsional deformations rapidly diffuse through

the structure. As the simulation proceeds, $|Tw|$ quickly assumes an approximately constant value as the structure becomes maximally torsionally deformed in the continued presence of the applied torque and thermal fluctuations. Plots of Tw versus position along the substructures, averaged over each of the first 25 1-μs time intervals (data not shown), confirm that twist diffuses rapidly from the end at which it is applied, quickly achieving an approximately homogeneous spatial distribution, as expected from the assumption that the bead-chain behaves as a homogeneous, linearly elastic filament characterized by isotropic twisting and bending.

At about 8 μs in $\mathcal{S}^-$, and at about 17 μs in $\mathcal{S}^+$, a mechanical threshold is reached, and buckling occurs. This is apparent in Fig. 3, where a relatively steep increase in $|Wr|$ coincides with a noticeable separation of the Tw and Lk curves. The outcome of these supercoiling events can be seen in the lower substructure in Fig. 2*c* and the upper substructure in Fig. 2*e*, respectively. The difference in time of onset for these transitions in $\mathcal{S}^-$ and $\mathcal{S}^+$ is a consequence of the stochastic

variability inherent in the solvated system. The average value of Lk from 8–9 μs in $\mathcal{S}^-$ is -1.50±0.014, and from 17–18 μs in $\mathcal{S}^+$ is 1.39±0.011. For the sake of comparison, we note that the onset of nonplanar bending of a circular, mechanically symmetric elastic rod *in vacuo* is expected to occur for $|\Delta Lk| \geq \frac{A\sqrt{3}}{C}$, independent of the length or thickness of the rod, or the Young's modulus of the material of which it is composed [31, 32]. In this expression, A and C are the bending and torsional rigidities, respectively. For the choices of parameter values used in this work, we calculate this threshold value as $|\Delta Lk| = 1.42$—in approximate agreement with the values of $|\Delta Lk|$ at which buckling is observed to occur. Prior to 25 μs, another buckling event occurs in each subdomain, as the imposed stress is partitioned almost exclusively as writhe, with twist remaining approximately constant. The crossings associated with these second events can be seen in Fig. 2*f* for $\mathcal{S}^+$, and Fig. 2*e* and *f* for $\mathcal{S}^-$. $|Wr|$ ultimately surpasses $|Tw|$ in both subdomains. At $t = 25\ \mu s$, we calculate $Lk^+ = Tw^+ + Wr^+ = 0.8348 + 1.478 = 2.313$ in

$\mathcal{S}^+$, and $Lk^- = Tw^- + Wr^- = -0.9359 - 1.526 = -2.462$ in $\mathcal{S}^-$. Ultimately, both substructures become maximally supercoiled, with Wr too assuming an approximately constant value after about 25 μs in both subdomains, as the molecule reaches mechanical equilibrium with the torsional load. Fig. 3 shows there is somewhat more fluctuation in $\mathcal{S}^+$ than in $\mathcal{S}^-$. For the time interval 25 to 100 μs, we calculate the average values: $<Tw^+>= 0.9315 \pm 0.00149$, $<Wr^+>= 1.408 \pm 0.00214$, $<Tw^->= -0.9759 \pm 0.00147$, and $<Wr^->= -1.570 \pm 0.00123$. The average value of the linking number for the *entire* structure, calculated over 100 μs, is $Lk = -0.2731$. Comparing this number with the values $|Lk| > 2.0$ for the individual subdomains confirms the implication of the twin supercoiling model that linking number measurements of an entire DNA ring or loop may not be good indicators of potentially important, stress-dependent biological events within its substructures.

The results of the writhe density calculations are plotted in Figs. 4 and 5. Fig. 4 corresponds to $\mathcal{S}^-$, the negatively

supercoiled subdomain (beads 1 to 25), and Fig. 5 to $\mathcal{S}^+$, the positively supercoiled subdomain (beads 26 to 50). Beads 25 and 50 are not represented in the figures, since no axis vector, $\mathbf{r}_{i+1} - \mathbf{r}_i$, is defined for them, and therefore no writhe can be caluculated (see Eq. (10)). The surfaces in Parts *a*–*d* of each figure are constructed from values of the argument in Eq. (10), plotted for each bead pair, and averaged over 1-μs time intervals from the first 25 μs of the simulation. The contours in the base planes of the figures are two-dimensional projections of the surfaces. Time intervals and contour elevations are indicated. In both subdomains, the time-averaged writhe, $<Wr>$, is initially approximately zero for all pairs, and the surfaces exhibit little deformation (Part *a* in both figures). As the simulation proceeds, and the imposed superhelicity is increasingly partitioned as writhe, the surfaces begin to "ripple" symmetrically, as shown in Part *b* of the figures. As expected from inspection of Fig. 3, during the 8-9 μs time interval in $\mathcal{S}^-$, and the 17-18 μs time interval in $\mathcal{S}^+$, noticeable peaks form in the writhe surfaces as the buckling threshold is

passed. These peaks then grow in magnitude until the structure absorbs a maximal amount of writhe, and the mechanical equilibrium mentioned above is reached. Figs. 4*d* and 5*d* are plots of the $\mathcal{S}^-$ and $\mathcal{S}^+$ writhe surfaces, respectively, for the interval 24 to 25 μs. It can be seen from the contour maps in this interval that the peaks have grown and bifurcated in both cases. Each region of bifurcation corresponds to a crossing of maximal writhe. The bead pairs associated with these crossings and the corresponding $<Wr>$ values are, for $\mathcal{S}^-$, $\{5, 23\} = -0.05325$ and $\{9, 19\} = -0.05721$, and for $\mathcal{S}^+$, $\{29, 47\} = 0.04857$ and $\{34, 44\} = 0.06520$. These crossings in turn correspond to locations on the helix axis that have come into contact as a result of the supercoiling that has occurred by this time; *i.e.*, precisely the two members of each associated bead pair make physical contact at the crossings visible in Fig. 2*f*.

The $\sigma^{+/-}$ calculations (data not shown) reveal that the superhelix densities at which the first buckling events occur, near 8 μs in $\mathcal{S}^-$ and 17 μs in $\mathcal{S}^+$, are -0.064 and 0.058, respec-

tively. By 25 μs, σ^+ rises to 0.11, and σ^- falls to -0.11, demonstrating that the superhelical stress generated by the modeled process is ample for producing localized transitions to secondary structures other than the B-form duplex, as predicted by the twin supercoiling model. We note that such transitions in typical transcriptional supercoiling domains occur under superhelical densities of only a few percent, and may take a minute or longer to stabilize [33], suggesting that the stress generated very rapidly here, though substantial, would need to be sustained in order to facilitate an event such as strand separation within the domain. This situation is a reflection of the relatively small size of the model domain (234 bp in each subdomain) in light of the length-dependence implicit in Eq. (12). Though nucleosome-free regulatory regions in eukaryotic genomes often involve only a few hundred basepairs, in typical prokaryotic transcriptional domains, encompassing thousands of basepairs, Lk_0 is proportionately larger, and the stress associated with deviations of Lk from Lk_0 proportionately smaller. We are currently extending our model for sim-

ulations involving larger domains. We finally note that the right-handedness of real B-DNA breaks the apparent symmetry of twin supercoiling. In particular, since the degree of overwinding (positive supercoiling) is restricted, typically only underwinding (negative supercoiling) generates superhelical stress sufficient to induce localized transformations of secondary structure; indeed, all well-characterized alternate structures are underwound relative to B-DNA.

The simulation results represented by Figs. 2–5 demonstrate that our model reproduces the Fig. 1 scenario, capturing several outstanding qualitative features of twin supercoiling, including: 1) superhelical deformations are negative in one portion of the twin domain and positive in the other; 2) the stress associated with these deformations is sufficient for driving biologically significant secondary structural transitions; and 3) experimental measurements of the linking number may not be an adequate indicator of the *in vivo* topological state of the domain, because it contains regions supercoiled to different degrees, and possibly even with opposite

signs [6]. More generally, our results illustrate major features of the topological response of DNA to dynamically-applied torsional stress, and suggest the need for further investigation of nonequilibrium scenarios such as that studied here; for example, the scenario in which transcription drives oppositely supercoiled domains in the same plasmid into dynamic merger [13].

Conclusion

We have presented a computational framework for modeling the long-time conformational dynamics of extended (hundreds of basepairs or longer) regions of dsDNA in solution, subjected to localized, external torques, such as those exerted by bound proteins engaged in tracking processes. This framework was used to investigate the dynamic twin supercoiling of a 477 basepair domain of topologically constrained B-DNA in response to the time-dependent superhelical stress generated by prokaryotic RNA polymerase and associated factors during transcription. Our results confirm several predictions of the twin supercoiling model, and elucidate a number of

characteristic features of nonequilibrium processes in which the topology of initially torsionally relaxed DNA is dynamically altered in the presence of solvent by a continually applied driving torque. These features include: 1) superhelical stress manifests principally as torsional deformation at early times, as imposed twist propagates through the structure; 2) thereafter, an approximately constant amount of evenly distributed twist is maintained, and the imposed stress manifests as a slow rise in writhe, until localized buckling results in plectonemic supercoiling; 3) the introduced stress continues to be apportioned approximately exclusively as writhe, resulting in additional supercoiling, until 4) the structure ultimately reaches mechanical equilibrium with the torsional load, and writhe too is maintained at a level approximately constant on average out to late times. These results suggest that transcription can potentially generate substantial superhelical stress very rapidly, illustrating the importance of DNA topology in gene regulation, and prompting further study of nonequilibrium processes that dynamically alter that topol-

ogy. Issues for future investigation include the roles played by thermal fluctuations and domain length in determining the time and location of onset of supercoiling, and the duration of approach to mechanical equilibrium. The present framework is currently being extended to model alternative transcriptional supercoiling scenarios involving several kilobasepair DNA domains, in which protein-DNA interactions are explicitly represented.

Acknowledgements

S.P. Mielke acknowledges the University of California, Lawrence Livermore National Laboratory and UC Davis, for continuing support through the Student Employee Graduate Research Fellowship (SEGRF). This work was performed under the auspices of the U.S. Department of Energy by the University of California, Lawrence Livermore National Laboratory, under Contract No. W-7405-Eng-48.

References

[1] Cozzarelli, N.R. & Wang, J.C., eds. (1990) *DNA Topology and Its Biological Effects* (Cold Spring Harbor Laboratory Press, Cold Spring Harbor).

[2] White, J. (1969) *Amer. J. Math.* **91**, 693–728.

[3] Nelson, P. (1999) *Proc. Natl. Acad. Sci. USA* **96**, 14342–14347.

[4] Benham, C.J. (1992) *J. Mol. Biol.* **225**, 835–847.

[5] Craig, N.L. (1988) *Annu. Rev. Genet.* **22**, 77–105.

[6] Liu, L.F. & Wang, J.C. (1987) *Proc. Natl. Acad. Sci. USA* **84**, 7024–7027.

[7] Wang, J.C. & Giaever, G.N. (1988) *Science* **240**, 300–304.

[8] Wang, J.C. (1988) *Harvey Lect.* **81**, 93–110.

[9] Wang, J.C. & Liu, L.F. (1990) in *DNA Topology and Its Biological Effects* (Cold Spring Harbor Laboratory

Press, Cold Spring Harbor), Cozzarelli, N.R. & Wang, J.C., eds., 321–340.

[10] Wang, J.C. (1996) *Annu. Rev. Biochem.* **65**, 635–692.

[11] Opel, M.L. & Hatfield, W. (2001) *Mol. Microbiol.* **39**, 191–198.

[12] Leng, F. & McMacken, R. (2002) *Proc. Natl. Acad. Sci. USA* **99**, 9139–9144.

[13] Stupina, V.A. & Wang, J.C. (2004) *Proc. Natl. Acad. Sci. USA* **101**, 8608–8613.

[14] Allison, S., Austin, R. & Hogan, M. (1989) *J. Chem. Phys.* **90**, 3843–3854.

[15] Chirico, G. & Langowski, J. (1994) *Biopolymers* **34**, 415–433.

[16] Huang, J. & Schlick, T. (2002) *J. Chem. Phys.* **117**, 8573–8586.

[17] Wang, M., *et al.* (1998) *Science* **282**, 902–907.

[18] Gunsteren, W.F. van, Berendsen, H.J.C. & Rullmann, J.A.C. (1981) *Molec. Phys.* **44**, 69–95.

[19] Chirico, G. (1996) *Biopolymers* **38**, 801–811.

[20] Merlitz, H., Rippe, K., Klenin, K.V. & Langowski, J. (1998) *Biophys. J.* **74**, 773–779.

[21] Varsalovich, D.A., Moskalev, A.N. & Khersonskii, V.K. (1988) *Quantum Theory of Angular Momentum* (World Scientific, Singapore).

[22] Ermak, D.L. & McCammon, J.A. (1978) *J. Chem. Phys.* **69**, 1352–1360.

[23] Hagerman, P.J. & Zimm, B.H. (1981) *Biopolymers* **20**, 1481–1502.

[24] Calladine, C.R. & Drew, H.R. (1997) *Understanding DNA* (Academic Press, San Diego).

[25] Lodish, H., *et al.* (2000) *Molecular Cell Biology, Fourth ed.* (W.H. Freeman and Company, New York).

[26] Dickinson, E., Allison, S.A. & McCammon, J.A. (1985) *J. Chem. Soc. Faraday Trans. 2* **81**, 591–601.

[27] Kubo, R. (1966) *Rep. Prog. Phys.* **29**, 255–284.

[28] Luby-Phelps, K. (2000) *Int. Rev. Cytol.* **192**, 189–221.

[29] Press, W.H., *et al.* (1997) *Numerical Recipes in C, Second ed.* (Cambridge University Press, Cambridge).

[30] Humphrey, W., Dalke, A. & Schulten, K. (1996) *J. Molec. Graphics* **14**, 33–38.

[31] Le Bret, M. (1979) *Biopolymers* **18**, 1709–1725.

[32] Benham, C.J. (1989) *Phys. Rev. A* **39**, 2582–2586.

[33] Peck, L.J. & Wang, J.C. (1983) *Proc. Natl. Acad. Sci. USA* **80**, 6206–6210.

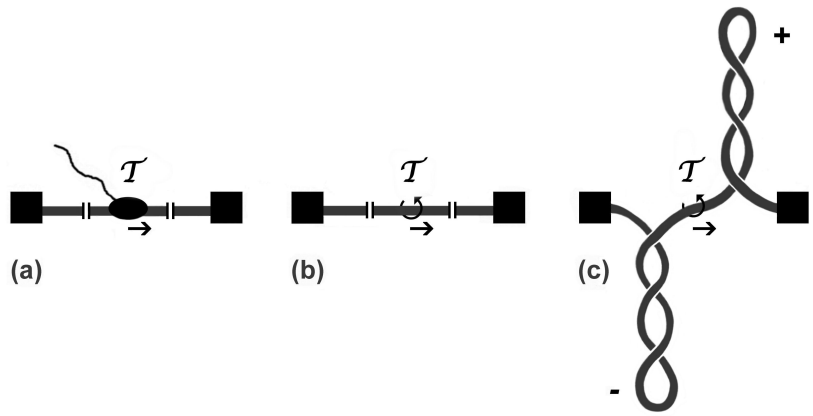

Figure 1: Twin supercoiling model (adapted from Ref. [6]). (a) A transcription ensemble, $\mathcal{T}$, tracks along a linear ds-DNA template from left to right. The ends of the DNA are anchored to large cellular structures, indicated by the solid squares. (b) Assuming rotation of $\mathcal{T}$ is hindered, for example due to viscous drag, a supercoiling torque is generated, and the template is "cranked" at the location of $\mathcal{T}$, represented by the circular arrow in the middle of the figure. (c) Because the structure is topologically constrained, torque upon the template at $\mathcal{T}$ generates superhelical stress, producing positive supercoils downstream, and negative supercoils upstream, from transcription.

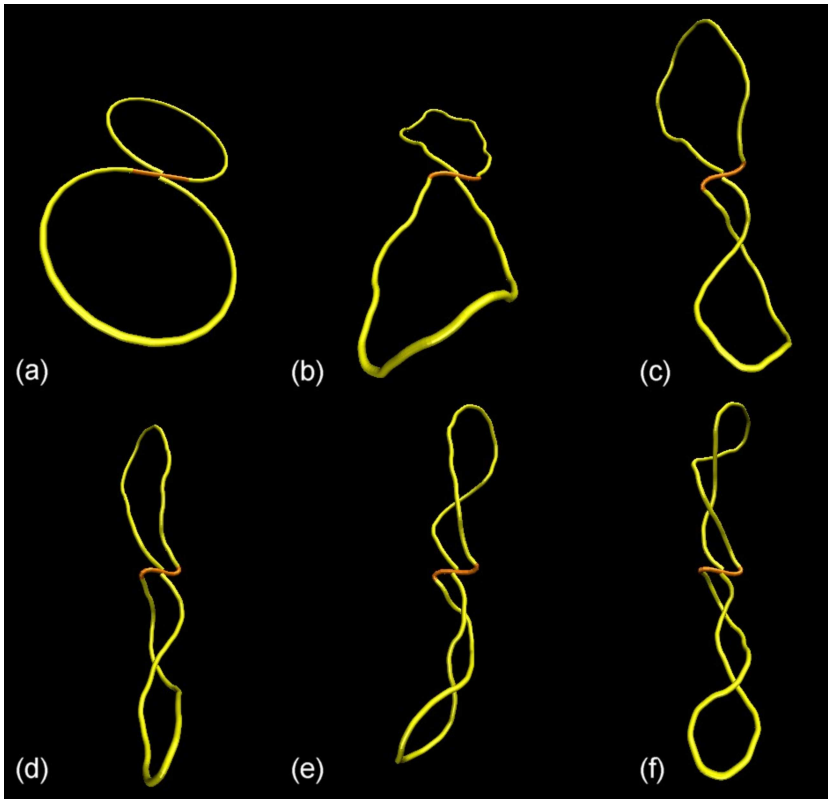

Figure 2: 25 μs trajectory. Both yellow substructures are initially torsionally relaxed. The orange segment corresponds to $\approx$18 bp—about the extent of the prokaryotic transcription bubble. The upper substructure ($\mathcal{S}^+$) becomes positively supercoiled, and the lower substructure ($\mathcal{S}^-$) negatively supercoiled, in response to an external torque applied over the course of the simulation. The spatial distribution of the torque extends over the first $\approx$37 bp of each subdomain, starting from the ends of the bubble. Altogether, the RNAP "footprint" spans a region of $\approx$92 bp at the center of the structure. The orientation and scale of the image are adjusted slightly in each frame to provide the most easily visualized perspective. (*a*) 0 μs. (*b*) 5 μs. (*c*) 10 μs. (*d*) 15 μs. (*e*) 20 μs. (*f*) 25 μs.

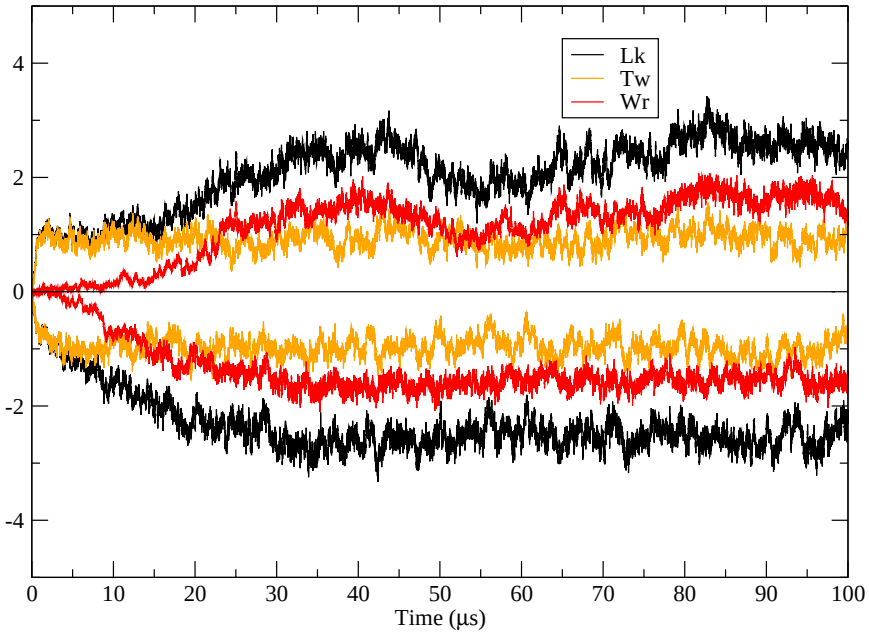

Figure 3: Linking number (Lk), twist (Tw), and writhe (Wr) from 0 to 100 μs. Superhelical deformations are positive in one half of the domain and negative in the other. Buckling is seen to occur at approximately 8 μs in $\mathcal{S}^-$ and 17 μs in $\mathcal{S}^+$, where there is noticeable separation of the Lk and Wr curves. All quantities remain nearly constant on average after approximately 25 μs.

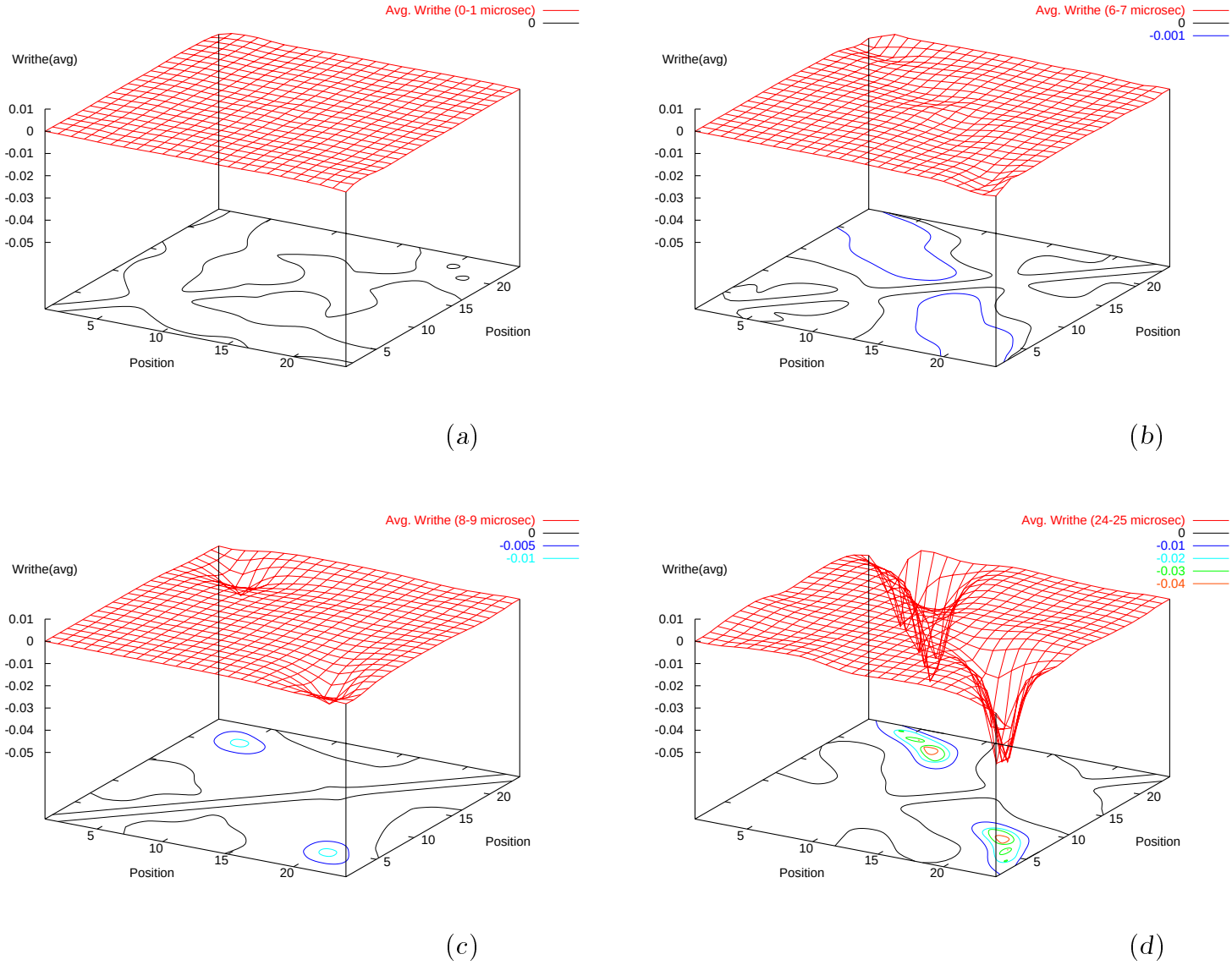

Figure 4: Time-averaged writhe densities for $\mathcal{S}^-$ from 0–25 μs: (a) 0–1 μs; (b) 6–7 μs; (c) 8–9 μs; (d) 24–25 μs. Contours in the base planes are 2-D projections of the writhe surfaces, with elevations indicated. The buckling event evident in c leads to a plectonemically supercoiled structure, represented in d, where the crossings of maximal writhe are $\{5, 23\} = -0.05325$ and $\{9, 19\} = -0.05721$ (see contour map). These crossings correspond to locations of self-contact in the structure at 25 μs (refer to discussion and Fig. 2f).

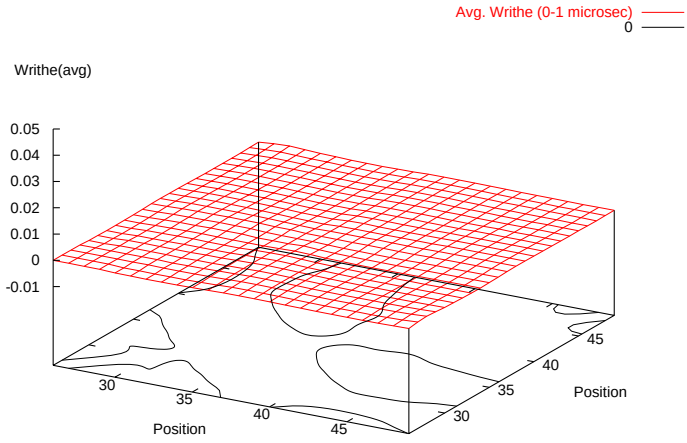

(a)

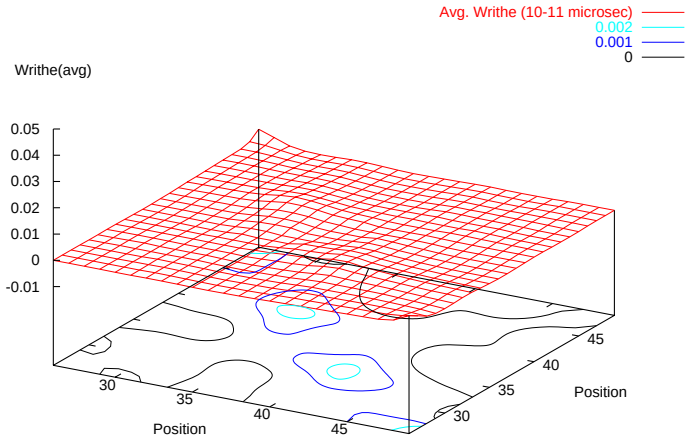

(b)

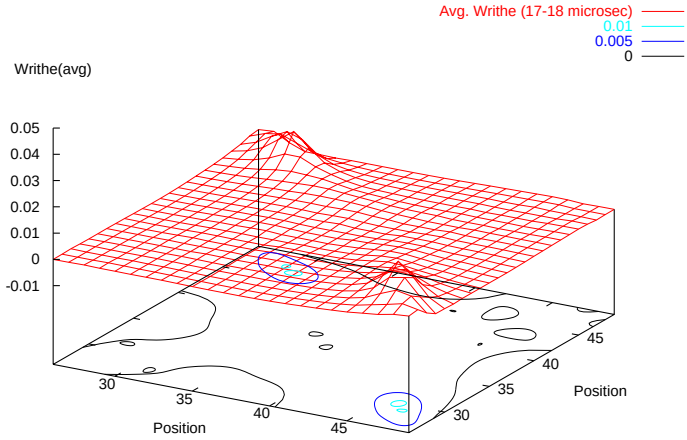

(c)

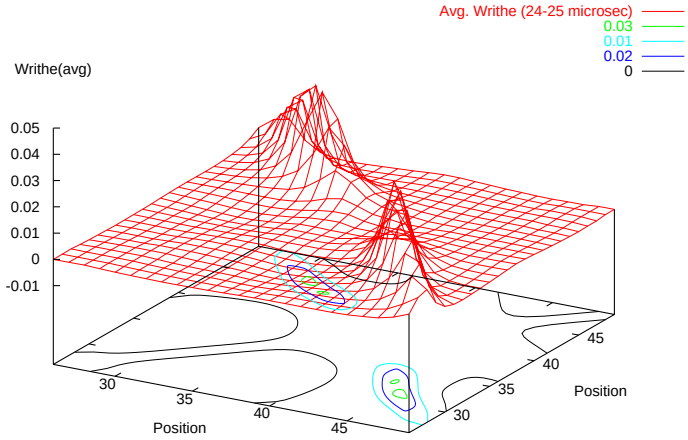

(d)

Figure 5: Time-averaged writhe densities for $\mathcal{S}^+$ from 0–25 μs: (a) 0–1 μs; (b) 10–11 μs; (c) 17–18 μs; (d) 24–25 μs. Contours in the base planes are 2-D projections of the writhe surfaces, with elevations indicated. The buckling event evident in c leads to a plectonemically supercoiled structure, represented in d, where the crossings of maximal writhe are $\{29, 47\} = 0.04857$ and $\{34, 44\} = 0.06520$ (see contour map). These crossings correspond to locations of self-contact in the structure at 25 μs (refer to discussion and Fig. 2f).